One-pot Synthesis of Helical Azaheptalene and Chiroptical Switch with Isolable Radical Cation

Yuta Nishimura, Takashi Harimoto, Takanori Suzuki and Yusuke Ishigaki*
Department of Chemistry, Faculty of Science
Hokkaido University
N10 W8, North-ward, Sapporo 060-0810, Japan
E-mail to corresponding author: yishigaki@sci.hokudai.ac.jp (Y.I.)

Abstract: A nitrogen-centered heptalene, azaheptalene, was designed as a representative of a new class of redox-responsive molecules with a large steric strain that originates from the adjacent seven-membered rings. The pentabenzo derivative of azaheptalene was efficiently synthesized by a palladium-catalyzed one-pot reaction of commercially available reagents. Bromination led to mono- and dibrominated derivatives, the latter of which is interconvertible with isolable radical cation species exhibiting near-infrared absorption. Since the azaheptalene skeleton shows configurationally stable helicity with a large torsion angle, enantiomers could be successfully separated. Thus, optically pure azaheptalenes with *P*- or *M*-helicity showed strong chiroptical properties ($|g_{abs}| \geq 0.01$), which could be changed by an electric potential.

Graphical Abstract:

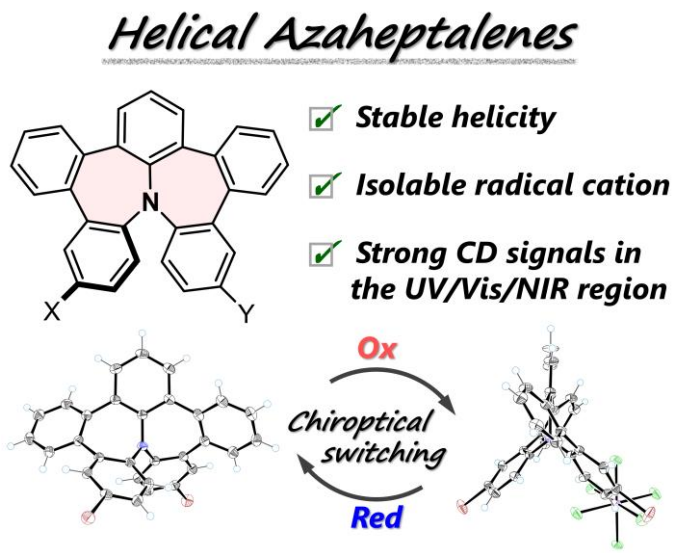

Heptalene **A**[1] is a representative nonalternant hydrocarbon, which is an attractive family of π-conjugated carbocycles involving odd-membered rings.[2–5] While open-shell and antiaromatic properties have been investigated for heptalene derivatives with a planar geometry,[6] heptalene **B**, in general, is a nonaromatic compound due to a potentially distorted structure derived from the seven-membered ring.[7] Based on this semi-rigid and nonplanar conformation of the seven-membered ring, multiple conformers can exist by introducing appropriate substituents on the heptalene skeleton. Indeed, the chiroptical properties of heptalene derivatives **B'** have been investigated by Hafner *et al*.[8] Furthermore, a seven-membered ring as seen in heptalene has been widely used to construct distorted molecules with unique properties;

negatively curved nanographenes[9–18] and highly strained molecules[19–22] have been reported within the past decade.

With regard to these intriguing characteristics caused by the seven-membered ring, several groups have focused on helical molecules with seven-membered rings and revealed their intrinsic properties.[23–28] Takasu *et al*. reported that a helical nanographene **C** composed of a contiguous 6-7-7-6 ring system has a large racemization barrier (ΔE_{calc} [B3LYP/6-31G(d,p)] = 29.2 kcal mol^{-1}) (Figure 1).[25] They were able to isolate an enantiopure isomer and revealed that such heptalene-embedded helical nanographene **C** exhibits strong circular dichroism (CD), whereas [4]helicene with a 6-6-6-6 ring system easily undergoes racemization due to its much lower energy barrier (ΔE_{calc} = 4.0 kcal mol^{-1}).[29,30] Thus, helical nanographene **C** with a heptalene skeleton can achieve configurational stablitity, which is quite rare.

We envisaged that if a similar helical structure could be synthesized more easily, we could obtain advanced molecules, the physical properties of which could be finely tuned by introducing substituents and/or switched by applying external stimuli. Herein, we report the first example of nitrogen (N)-centered helical heptalene **1** (Figure 1), where the azaheptalene skeleton can be constructed by a palladium-catalyzed one-pot reaction. Thanks to the electron-donating ablity of the central nitrogen atom, electrophilic bromination of **1** proceeds easily to produce mono- and dibrominated azaheptalene derivatives **2** and **3**, and these azaheptalenes all undergo one-electron oxidation to give the corresponding radical cation species. Furthermore, due to the contiguous 6-7-7-6 ring system, these N-doped heptalenes gain configurational stability, so that not only photophysical properties but also chiroptical properties can be controlled by an electric potential.

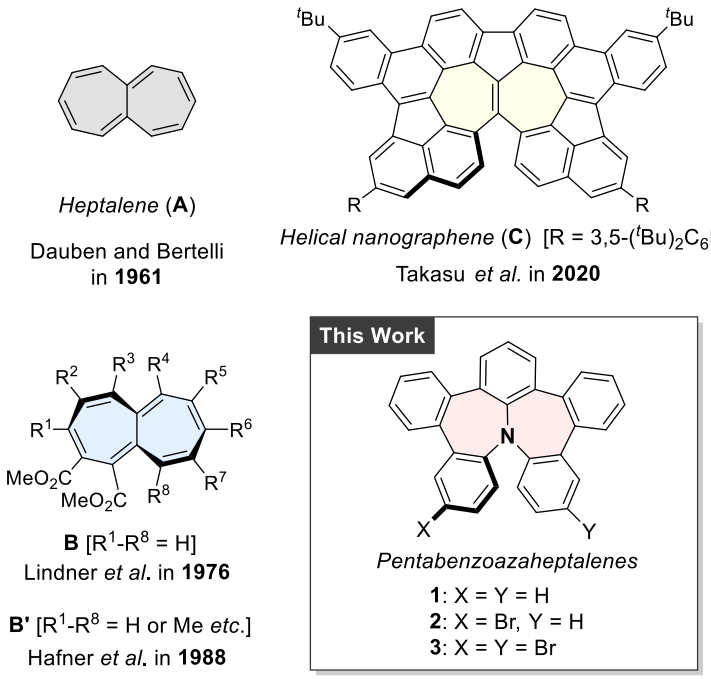

Figure 1. Heptalene derivatives: previous examples and this study.

Pentabenzoazaheptalene **1** was synthesized by a one-pot reaction (y. 82%) via Buchwald-Hartwig amination of 2,2'-dibromobiphenyl and 9*H*-tribenzo[*b*,*d*,*f*]azepine[31] followed by the palladium-catalyzed C-C bond formation (Scheme 1).[32] Due to the electron-donating nitrogen atom, selective bromination of **1** proceeded cleanly. By treatment of **1** with one equivalent of NBS and three equivalents of Br_2, mono- and dibrominated derivatives **2** and **3** were obtained in 53% and 86% yields, respectively. During these reactions, overbrominated compound was not found because of the lower contribution of HOMO on the benzene ring at the center of the molecule compared to the contributions of those on both sides (Figure S5).

Scheme 1. Preparation of azaheptalene derivatives **1**–**3**.

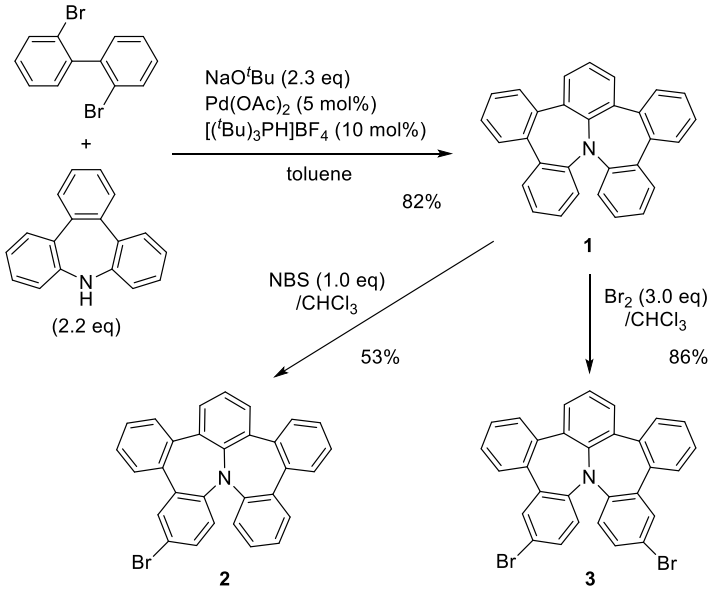

These azaheptalenes **1**–**3** were characterized by NMR spectroscopy and mass spectrometry and finally determined by single-crystal X-ray diffraction. X-ray analyses revealed that all azaheptalenes **1**–**3** adopt a highly distorted geometry with a dihedral angle [θ/° = 103.89(11) for **1**, 103.9(6) and 102.1(7) for **2**, and 100.3(5) for **3**, respectively] between benzene rings on both sides (Figure 2a-c). These values were well-reproduced in optimized structures [θ/° = 104.0 for **1**, 103.9 for **2**, and 103.9 for **3**, respectively] by density functional theory (DFT) calculations at the B3LYP/6-31G(d,p) level (Figure S7). Since the dihedral angle θ of helical nanographene **C** is 57.51(3) °,[25] these helical azaheptalenes with much larger angles are expected to have higher racemization barriers to enable the successful isolation of both enantiomers of these azaheptalenes (*vide infra*).

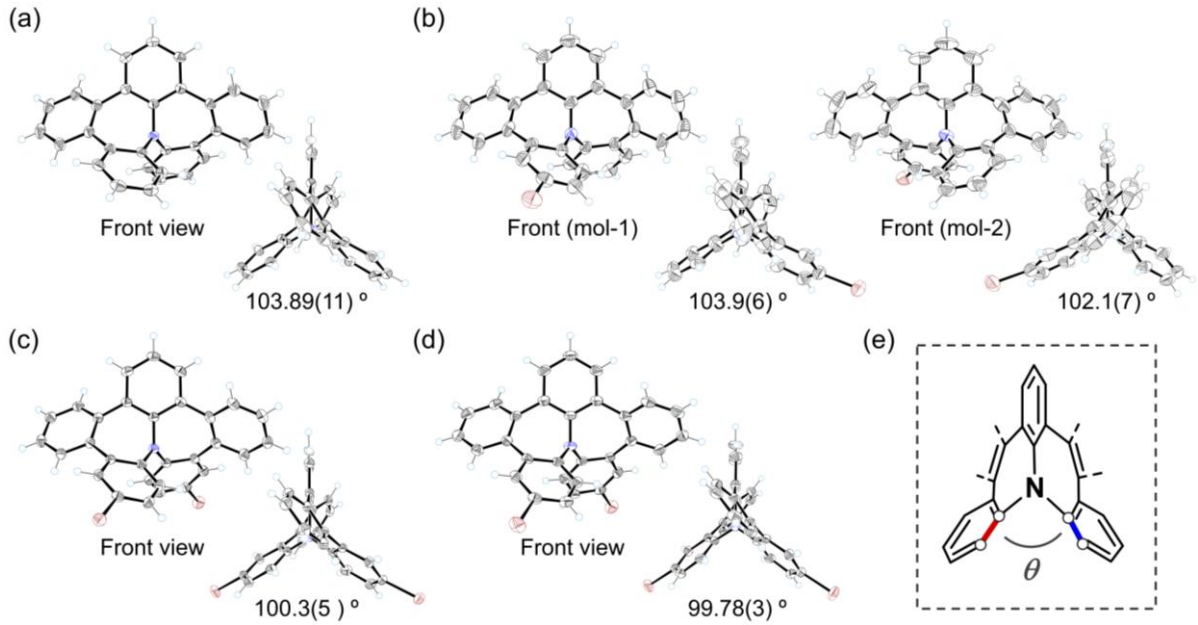

Figure 2. X-ray structures of (a) **1**, (b) **2** (two crystallographically independent molecules), (c) **3**, and (d) (*P*)-**3**. Thermal ellipsoids are shown at the 50% probability level. (e) The dihedral angle θ was defined as the torsion of two C-C bonds. Disordered atoms are omitted for clarity for **2**.

To investigate the redox properties of these azaheptalenes **1**–**3**, we conducted cyclic voltammetry in CH_2Cl_2. A reversible one-electron oxidation wave was observed for all derivatives (Figure 3a), whereas both parent triphenylamine and *N*-phenyl tribenzoazepine[33] gave an irreversible oxidation wave (Figure S11). These results indicate that double ethenylene bridges certainly contribute to the stability of radical cation species. Next, we generated radical cation salts of these azaheptalenes. In fact, by treatment of dibromoazaheptalene **3** with one equivalent of $(2,4\text{-}Br_2C_6H_3)_3N^{+\bullet}SbCl_6^-$ (Magic Green),[34] $\mathbf{3}^{+\bullet}SbCl_6^-$ was isolated in 79% yield as a dark green powder (Figure 3b). The structure of radical cation $\mathbf{3}^{+\bullet}$ was determined by X-ray analysis, where the dihedral angle θ decreased from 100.3(5) ° to 92.95(10) ° upon oxidation (Figure 3c). The decrease in the dihedral angle can be accounted for by an effective delocalization of the spin and positive charge over the whole molecule. For non- and monobrominated derivatives **1** and **2**, a generated radical cation was too reactive to be isolated. These results indicate that the introduction of bromine atoms into reactive sites is more effective for kinetic stabilization of radical cation species despite its electron-withdrawing properties ($E_{1/2}$/V vs SCE: +1.39 for **1**, +1.45 for **2**, and +1.51 for **3**).

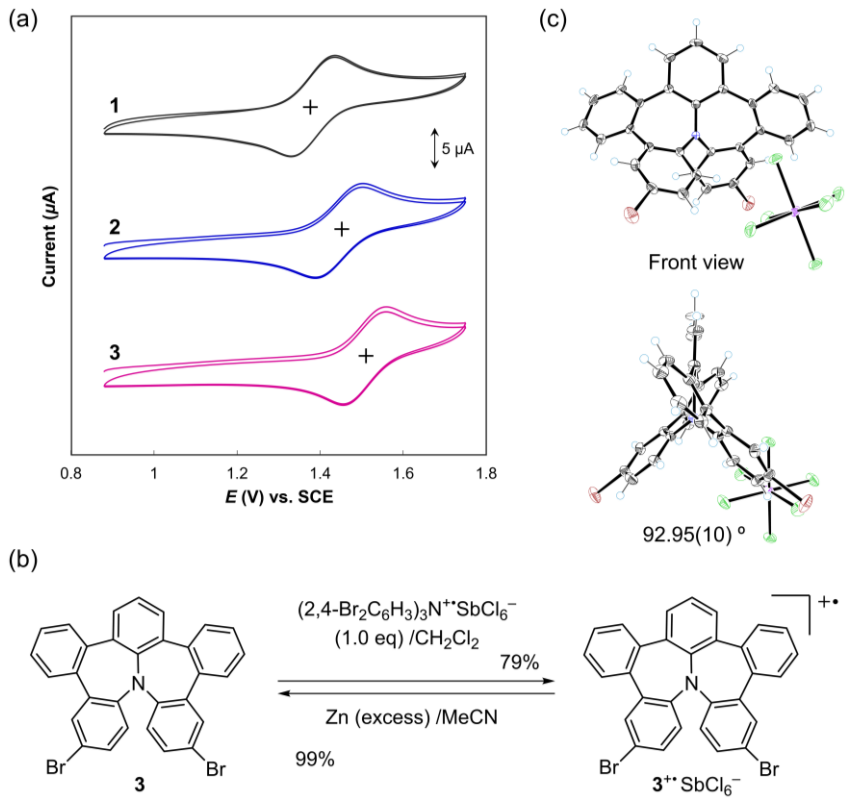

Figure 3. (a) Cyclic voltammograms of **1**–**3** (1.0 mM) at 297 K in CH_2Cl_2 containing 0.1 M Bu_4NBF_4 as a supporting electrolyte (scan rate 0.1 V s^{-1}, Pt electrodes). (b) Redox interconversion between **3** and **3**$^{+\bullet}SbCl_6^-$. (c) X-ray structure of **3**$^{+\bullet}SbCl_6^-$. Thermal ellipsoids are shown at the 50% probability level.

With both neutral and radical cation species of **3** in hand, we next measured absorption spectra in CH_2Cl_2. While neutral dibromoazaheptalene **3** exhibited absorptions only in the UV region, radical cation **3**$^{+\bullet}$ showed broad absorptions over the visible and near-infrared (NIR) regions (Figure 4a,b and Table 1). For neutral **3**, the first band was assigned to the n-π* transition, and the UV spectrum was almost identical regardless of the presence or absence of bromine atom. In the case of radical cation **3**$^{+\bullet}$, a NIR absorption band extending to 1600 nm was observed, which mainly arises from the SOMO-NHOMO transition. These results were supported by time-dependent (TD)-DFT calculations (Figure S9).

Table 1. UV/Vis/NIR and CD spectral data measured in CH_2Cl_2.

	λ_{max}/nm (log ε)	λ_{ext}/nm ($\Delta\varepsilon$)
1	320 (3.64), 262 (4.57), 236 (4.85)	(*P*): 329 (–17.5), 286 (–32.9), 260 (+186) (*M*): 327 (+17.1), 286 (+32.3), 260 (–183)
2	320 (3.62), 263 (4.56), 237 (4.84)	(*P*): 329 (–25.1), 291 (–29.9), 261 (+180) (*M*): 328 (+24.4), 291 (+29.3), 261 (–176)
3	321 (3.61), 263 (4.60), 237 (4.84)	(*P*): 330 (–30.8), 295 (–37.2), 262 (+191) (*M*): 331 (+30.6), 294 (+36.8), 262 (–189)
3$^{+\bullet}SbCl_6^-$	889 (3.62), 654 (3.67), 263 (4.63), 235 (4.82)	(*P*): 904 (–4.6), 561 (+1.4), 395 (–8.6), 315 (–17.9), 279 (+66.5), 261 (+120) (*M*): 906 (+4.2), 563 (–1.1), 392 (+9.1), 314 (+18.5), 279 (–64.7), 260 (–115)

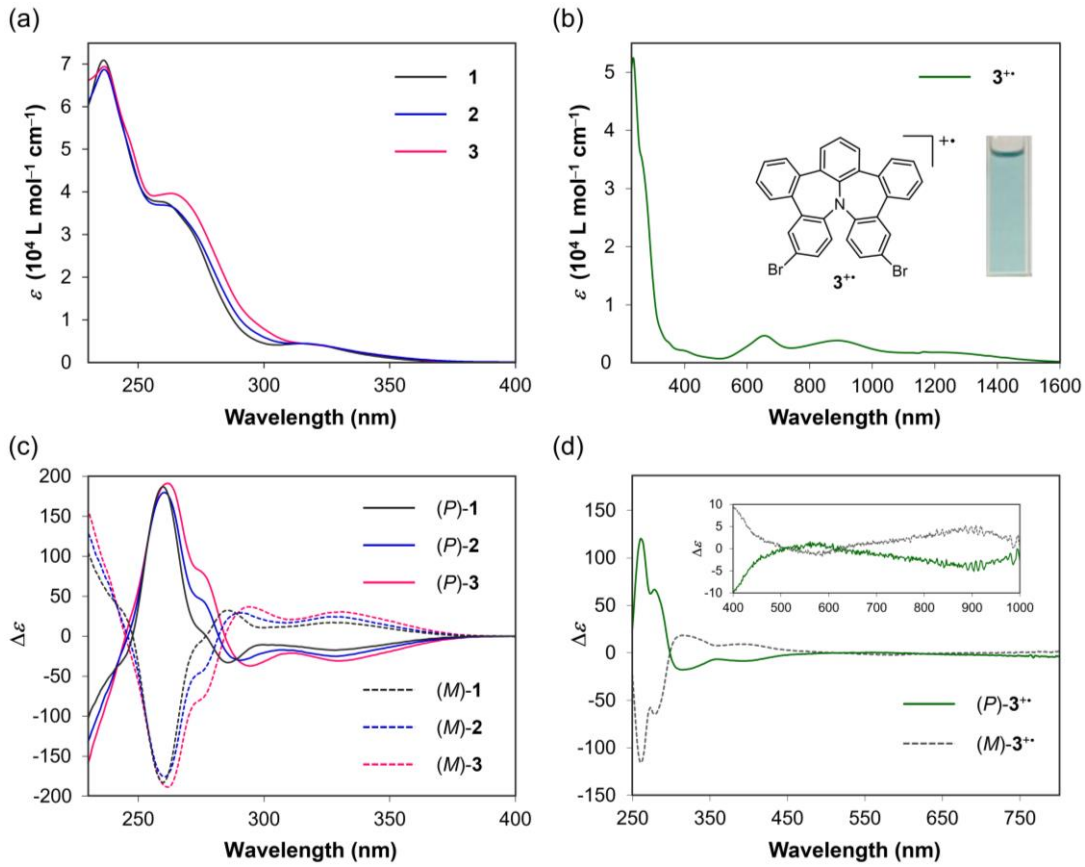

Figure 4. (a) UV spectra of **1**–**3** and (b) UV/Vis/NIR spectrum of **3**$^{+\bullet}$$SbCl_6^-$ in CH_2Cl_2. CD spectra of enantiomers of (c) neutral azaheptalenes **1**–**3** and (d) **3**$^{+\bullet}$$SbCl_6^-$ in CH_2Cl_2.

To elucidate the chiroptical properties of these helical azaheptalenes, we carried out chiral separation. All azaheptalenes **1**–**3** could be separated by chiral HPLC on a Daicel CHIRALPAK IG (Chart S1). The 1st fraction exhibited a minus value of optical rotation (see SI), and the absolute configuration was finally determined to be *P*-helicity by X-ray analysis of **3** [Flack parameter: χ = –0.060(10)] (Figure 2d). The dihedral angle θ of (*P*)-**3** is 99.78(3) °, which is almost the same as that of (*rac*)-**3**. CD spectra of (*P*)- and (*M*)-**1**–**3** in CH_2Cl_2 clearly show negative and positive first Cotton effects, respectively, and are well-reproduced by TD-DFT calculations (Figure S10). The CD spectral patterns are quite similar among **1**–**3** probably due to the rigidity of the helical azaheptalene skeleton. Notably, these helical azaheptalenes **1**–**3** exhibit high absorption dissymmetrical factors [$|g_{abs}$ (345 nm)| = 0.012 for **1**, 0.010 for **2**, and 0.013 for **3**] (Figures S12-14), which are much larger than those of helicene derivatives with a similar number of fused rings.[35,36] Furthermore, the chiroptical properties can be switched upon oxidation. Indeed, by treatment of (*P*)- and (*M*)-**3** with one equivalent of Magic Green, (*P*)- and (*M*)-**3**$^{+\bullet}$$SbCl_6^-$ were isolated in 42% and 52% yields, respectively. These radical cations with *P*- and *M*-helicity also displayed mirror-image CD spectra even in the NIR region.

Since racemization of (*P*)-**3** was too slow, the barrier was not experimentally determined (Figure S15). Thus, we performed DFT calculations and found that all azaheptalenes have much higher racemization barriers (ΔE_{calc}/kcal mol^{-1} = 50.5 for **1**, 50.7, for **2**, and 50.9 for **3**) (Figures 5 and S8) than those for helical nanographene with a 6-7-7-6 ring system (ΔE_{calc}/kcal mol^{-1} = 29.2)[25] and N-centered [4]helicene with a 6-6-6-6 ring system (ΔE_{calc}/kcal mol^{-1} = 32.7).[37] Thus, we concluded that the theoretically obtained barrier of ca. 50 kcal mol^{-1} is reasonable for these systems. In the case of radical cation **3**$^{+\bullet}$, DFT calculations [B3LYP/6-31G(d,p)] revealed a smaller racemization barrier (ΔE_{calc}/kcal mol^{-1} = 40.1 for **3**$^{+\bullet}$) (Figure S8c), which can be accounted for by the decreased torsion upon oxidation.

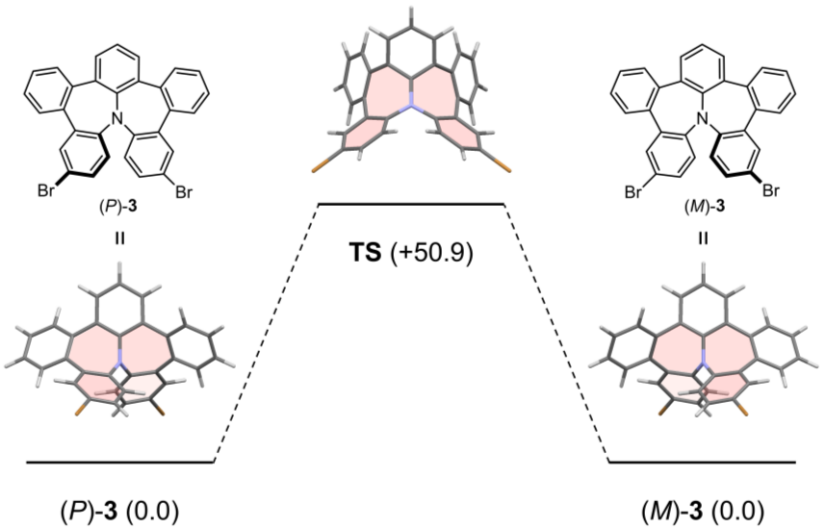

Figure 5. Computed racemization process of azaheptalene **3**.

In conclusion, we designed helical azaheptalenes **1**–**3** with a contiguous 6-7-7-6 ring system, which could be efficiently synthesized by a palladium-catalyzed one-pot reaction. Regardless of these azaheptalenes composed of a minimal number of fused rings, its helicity exhibits sufficient configurational stablity to be separated using chiral HPLC. Moreover, thanks to the electron-donating nitorogen atom, such helical azaheptalene **3** undergoes one-electron oxidation to produce radical cation species with a chiroptical response. Notably, a larger g_{abs} value was observed in the UV region for neutral azaheptalene **3** with *P* or *M* helicity, and its radical cation (*P*) or (*M*)-**3**$^{+\bullet}$$SbCl_6^-$ exhibited obvious CD signals extending to the NIR region. Therefore, helical azaheptalene, the chiroptical properties of which can be switched by an electric potential, may help to pave the way for the development of stimuli-responsive materials.

Acknowledgements

This work was supported by Grant-in-Aid from MEXT and JSPS (Nos. JP20H02719, JP21H01912, and JP23H04011). Y.I. acknowledges the Foundation of the Promotion of Ion Engineering.

Keywords: azaheptalene; helicity; radicals; cations; chiroptical response

References:

[1] H. J. Dauben, D. J. Bertelli, *J. Am. Chem. Soc.* **1961**, *83*, 4659–4660.

[2] T. Nozoe, *Topics in Nonbenzenoid Aromatic Chemistry*, Wiley, **1974**.

[3] Y. Tobe, *Chem. Rec.* **2015**, *15*, 86–96.

[4] A. Konishi, M. Yasuda, *Chem. Lett.* **2021**, *50*, 195–212.

[5] S. Moles Quintero, M. M. Haley, M. Kertesz, J. Casado, *Angew. Chem. Int. Ed.* **2022**, *61*, e202209138.

[6] A. Konishi, K. Horii, D. Shiomi, K. Sato, T. Takui, M. Yasuda, *J. Am. Chem. Soc.* **2019**, *141*, 10165–10170.

[7] H. J. Lindner, B. Kitschke, *Angew. Chem. Int. Ed. Engl.* **1976**, *15*, 106–107.

[8] K. Hafner, G. L. Knaup, H. J. Lindner, *Bull. Chem. Soc. Jpn.* **1988**, *61*, 155–163.

[9] K. Kawasumi, Q. Zhang, Y. Segawa, L. T. Scott, K. Itami, *Nat. Chem.* **2013**, *5*, 739–744.

[10] K. Y. Cheung, X. Xu, Q. Miao, *J. Am. Chem. Soc.* **2015**, *137*, 3910–3914.

[11] X. Gu, H. Li, B. Shan, Z. Liu, Q. Miao, *Org. Lett.* **2017**, *19*, 2246–2249.

[12] S. H. Pun, Q. Miao, *Acc. Chem. Res.* **2018**, *51*, 1630–1642.

[13] S. H. Pun, Y. Wang, M. Chu, C. K. Chan, Y. Li, Z. Liu, Q. Miao, *J. Am. Chem. Soc.* **2019**, *141*, 9680–9686.

[14] X. Yang, F. Rominger, M. Mastalerz, *Angew. Chem. Int. Ed.* **2019**, *58*, 17577–17582.

[15] K. Kato, K. Takaba, S. Maki-Yonekura, N. Mitoma, Y. Nakanishi, T. Nishihara, T. Hatakeyama, T. Kawada, Y. Hijikata, J. Pirillo, L. T. Scott, K. Yonekura, Y. Segawa, K. Itami, *J. Am. Chem. Soc.* **2021**, *143*, 5465–5469.

[16] S. Zank, J. M. Fernández‐García, A. J. Stasyuk, A. A. Voityuk, M. Krug, M. Solà, D. M. Guldi, N. Martín, *Angew. Chem. Int. Ed.* **2022**, *61*, e202112834.

[17] J. M. Fernández-García, P. Izquierdo-García, M. Buendía, S. Filippone, N. Martín, *Chem. Commun.* **2022**, *58*, 2634–2645.

[18] L. Yang, Y. Ju, M. A. Medel, Y. Fu, H. Komber, E. Dmitrieva, J. Zhang, S. Obermann, A. G. Campaña, J. Ma, X. Feng, *Angew. Chem. Int. Ed.* **2023**, *62*, e202216193.

[19] J. M. Farrell, V. Grande, D. Schmidt, F. Würthner, *Angew. Chem. Int. Ed.* **2019**, *58*, 16504–16507.

[20] Y. Ishigaki, Y. Hayashi, T. Suzuki, *J. Am. Chem. Soc.* **2019**, *141*, 18293–18300.

[21] T. Shimajiri, T. Suzuki, Y. Ishigaki, *Angew. Chem. Int. Ed.* **2020**, *59*, 22252–22257.

[22] A. Shimizu, T. Morikoshi, K. Sugisaki, D. Shiomi, K. Sato, T. Takui, R. Shintani, *Angew. Chem. Int. Ed.* **2022**, *61*, e202205729.

[23] J. Ma, Y. Fu, E. Dmitrieva, F. Liu, H. Komber, F. Hennersdorf, A. A. Popov, J. J. Weigand, J. Liu, X. Feng, *Angew. Chem. Int. Ed.* **2020**, *59*, 5637–5642.

[24] Y. Han, Z. Xue, G. Li, Y. Gu, Y. Ni, S. Dong, C. Chi, *Angew. Chem. Int. Ed.* **2020**, *59*, 9026–9031.

[25] N. Ogawa, Y. Yamaoka, H. Takikawa, K. Yamada, K. Takasu, *J. Am. Chem. Soc.* **2020**, *142*, 13322–13327.

[26] Z. Qiu, S. Asako, Y. Hu, C.-W. Ju, T. Liu, L. Rondin, D. Schollmeyer, J.-S. Lauret, K. Müllen, A. Narita, *J. Am. Chem. Soc.* **2020**, *142*, 14814–14819.

[27] C. Duan, J. Zhang, J. Xiang, X. Yang, X. Gao, *Angew. Chem. Int. Ed.* **2022**, *61*, e202201494.

[28] T. Ikai, K. Oki, S. Yamakawa, E. Yashima, *Angew. Chem. Int. Ed.* **2023**, *62*, e202301836.

[29] S. Grimme, S. D. Peyerimhoff, *Chem. Phys.* **1996**, *204*, 411–417.

[30] J. Barroso, J. L. Cabellos, S. Pan, F. Murillo, X. Zarate, M. A. Fernandez-Herrera, G. Merino, *Chem. Commun.* **2018**, *54*, 188–191.

[31] C. Cheng, D. Tu, X. Zuo, Z. Wu, B. Wan, Y. Zhang, *Org. Lett.* **2021**, *23*, 1239–1242.

[32] When 5*H*-dibenzo[*b*,*f*]azepine was used for the one-pot reaction, tetrabenzoazaheptalene was obtained in 48% yield, demonstrating the efficiency of this synthetic protocol.

[33] T. Hu, Z. Ye, K. Zhu, K. Xu, Y. Wu, F. Zhang, *Org. Lett.* **2020**, *22*, 505–509.

[34] W. Yueh, N. L. Bauld, *J. Am. Chem. Soc.* **1995**, *117*, 5671–5676.

[35] J. E. Field, G. Muller, J. P. Riehl, D. Venkataraman, *J. Am. Chem. Soc.* **2003**, *125*, 11808–11809.

[36] H. Nishimura, K. Tanaka, Y. Morisaki, Y. Chujo, A. Wakamiya, Y. Murata, *J. Org. Chem.* **2017**, *82*, 5242–5249.

[37] B. D. Gliemann, A. G. Petrovic, E. M. Zolnhofer, P. O. Dral, F. Hampel, G. Breitenbruch, P. Schulze, V. Raghavan, K. Meyer, P. L. Polavarapu, N. Berova, M. Kivala, *Chem. Asian J.* **2017**, *12*, 31–35.

[38] CCDC numbers 2265031-2265036.